Aerospace Science and Technology 93 (2019) 105333

Contents lists available at ScienceDirect

Aerospace Science and Technology

www.elsevier.com/locate/aescte

Dynamic analysis of stiffened bi-directional functionally graded plates with porosities under a moving load by dynamic relaxation method with kinetic damping

Mostafa Esmaeilzadeh [a], Mehran Kadkhodayan [b,*]

[a] Department of Mechanical Engineering, Mashhad Branch, Azad University, Mashhad, Iran
[b] Department of Mechanical Engineering, Ferdowsi University of Mashhad, Mashhad, Iran

ARTICLE INFO

Article history:
Received 6 February 2019
Received in revised form 26 June 2019
Accepted 8 August 2019
Available online 12 August 2019

Keywords:
Stiffened porous bi-directional FG plates
Moving loads
First order shear deformation theory
Dynamic relaxation method with kinetic damping
Newmark integration method

ABSTRACT

The principal purpose of this study is investigating the dynamic analysis of porous bi-directional functionally graded (FG) plates reinforced by eccentrically outside stiffeners and subjected to a moving load with a constant velocity. The materials are assumed to be graded in two directions and their effective properties are computed by the rule of mixtures. The FG plates are assumed to have both even and uneven distribution of porosities over the plate cross-section. Using appropriate kinematic relations, the displacements of the plate mid-plane are compatible with those of the stiffeners. The governing differential equations of porous bi-directional FG plates are derived through Hamilton's principle based on the first order shear deformation theory (FSDT) and Von Karman relations for large deflections. Moreover, dynamic relaxation method with kinetic damping (K-DR) coupled with Newmark integration technique are used to solve the plate's time-varying nonlinear equations. The effects of some numerical aspect ratios such as volume fraction, boundary conditions, porosity coefficients and distribution patterns and the existence of stiffeners on dynamic behaviors are investigated. The results show that the stiffness of the porous bi-directional FG plates is highly improved with the aid of eccentric stiffeners; hence, better dynamic behaviors are provided.

1. Introduction

In recent decades, a plethora of research have been conducted on manufacturing the plates which can be employed in the wide range of structures and engineering applications such as aerospace, marine structures, and automobiles [1]. Functionally graded materials (FGMs) are new type of materials introduced in 1984 [2], whose compositions are designed to change continuously within the body, particularly along the thickness direction [3–5]. In this case, nonlinear steady-state responses of an axially moving functionally graded plate coupled with ideal liquid was reported by Wang and Zu [6]. Duc et al. [7] dealt with dynamic behaviors of supported FGM plates under thermal and damping loadings. Another study on dynamic responses of piezoelectric sigmoid FG shells with cylindrical shape on elastic foundations and under thermal-electro-mechanical loading was performed by N.D. Duc [8]. As time goes by, modern structures and components may require advanced materials in which their constituents vary continuously in different directions [9]. To do this, bi-directional functionally graded materials (2D-FGMs) are introduced, which are of great importance in the design and development of engineering applications especially once more effective high-temperature resistant materials are compulsory. In contrast with one-directional FG materials, FGMs with two-dimensional dependent material properties can resist far more severe variations of temperature [10]. Until now, scholars have performed a number of studies on this field. In the following, these studies are reviewed briefly.

Li et al. [11] developed an algorithm based on differential quadrature method for the thermo-elastic analysis of bi-directional FGM plates. In the same year, 2009, Nemat-Alla et al. [12] used a 3D finite element model to numerically scrutinize the elastoplastic behaviors of 2D-FGMs under thermal loading. Some years later, the free vibration of a two-dimensional functionally graded circular cylindrical shell is analyzed by Ebrahimi and Najafizadeh [13]. Satouri et al. [14] undertook studies on elastic buckling analysis of a two-dimensional functionally graded cylindrical shell reinforced by axial stiffeners (stringer) under combined compressive axial and transverse uniform distributive loads using differential quadrature method (DQM). In this study, the effects of some items like loads, geometrical and stringer parameters along with FG power index on

* Corresponding author.
E-mail address: kadkhoda@um.ac.ir (M. Kadkhodayan).

https://doi.org/10.1016/j.ast.2019.105333
1270-9638/

the critical buckling load for different boundary conditions were investigated. Furthermore, the concept of 2D-FGMs was also applied to nano-structures [15,16].

There are several procedures to fabricate FGMs; for example, Powder Metallurgy [17], vapor deposition, multi-step sequential infiltration technique, non-pressure sintering technique and self-propagating high temperature synthesis technique [18]. Nevertheless, in the process of preparing FGMs, porosities and micro-voids may occur inside materials due to a few technical issues. For instance, the constrictions between adjacent compositions of metal and ceramic phases in functionally graded materials can arise during the sintering process, which may result in a number of porosities scattering inside the materials [19]. Additionally, when multi-step sequential infiltration technique is applied, it is hard to penetrate the secondary material into the middle area rigorously, whereas infiltrating the material into the top and bottom zones is easier, as a result of which, porosities happen mainly in the middle zone of the FGMs. Also, because of the large difference in solidification temperatures between material constituents, porosities or micro-voids can be formed during the process of sintering [20]. Some studies have been performed on the static and dynamic behavior of porous structures using the various theories of elasticity. The interaction of a fluid with a moving FG plate containing micro-voids was studied numerically by Wang and Yang [21]. Another study on vibration characteristics of porous FGM plates moving in a thermal environment was conducted by Wang and Zu [22]. Duc et al. [23] explored the effects of temperatures and mechanical loads on transient bending deflections of porous functionally graded plates based on the first order deformation theory. They demonstrated that temperature field and applied loads can impose great impacts on performances of FGM plates with porosities. Duc [24] also analytically studied the effects of porosity on dynamic responses of supported FGM shallow spherical shells reinforced with outside stiffeners. In another study, Duc and Quan [25] carried out an investigation into nonlinear mechanical responses of eccentrically stiffened FGM cylindrical panels containing porosities resting elastic foundations with the aid of Bubnov-Galerkin technique and a proper stress function. Ziane et al. [26] used an analytical method to predict the thermal buckling of FGM box beams. By means of a modified power law approach as well as D'Alembert's theory, Wang [27] investigated nonlinear dynamics of imperfect functionally graded piezoelectric plates in translation state. It was revealed that electric potential, FG gradient indices and translational velocity have considerable influences on natural frequency of structures. Taking Reddy's higher-order shear deformation plate theory into consideration, Cong et al. [28] studied buckling and post-buckling behavior of functionally graded plates with porosities resting on elastic foundations and subjected to mechanical, thermal and thermomechanical loads. In 2018, Wang et al. [29] carried out research on thermal vibration of a cylindrical shell with geometrical imperfections distributed evenly or unevenly through the thickness direction. Based on the first order shear deformation theory (FSDT), the elastic buckling and free vibration of plates with uniform and non-uniform porosity dispersions were analyzed by Thang et al. [30]. A detailed numerical study was conducted on the free vibration of porous FG plates supported by Winkler/Pasternak/Kerr foundations by Shahsavari et al. [31]. They used Galerkin method to solve the equations. The differential transformation method (DTM) was employed by Wattanasakulpong and Chaikittiratana [32] to investigate the linear and nonlinear vibration responses of porous FG beams elastically restrained at two ends on elastic supports. Recently, Tang et al. [33] concluded that the effect of porosity dispersed in the thickness direction on the critical buckling load is more noticeable compared to the impact of axial porosity distribution.

Solids under action of moving loads are employed in a wide variety of applications, such as machine tools, transportation and aerospace engineering. Relevant to such applications, Lamb was the first one who investigated wave propagation in a plate under a moving load [34]. Afterward, Wilson and Tsrik [35] analyzed the dynamic behavior of a rectangular plate and a cylindrical shell with various elasticity modulus. Based upon thin plate theory, Agrawal et al. [36] studied the dynamic response of orthotropic thin plates excited by moving masses. Applying superposition principle, Marchesiello et al. [37] improved a dynamic interaction model of vehicle-bridge and the bridge was displayed as an isotropic rectangular plate. De Faria and Oguamanam [38] proposed a new strategy based on an adaptive mesh scheme to investigate the vibration of Mindlin plates under traveling concentrated loads. In another study, Vosoughi et al. [39] analyzed dynamic response of a laminated plate on an elastic foundation under a moving load. High-order shear deformation theory and numerical differential quadrature method along with the Newmark method were adopted to solve the problem. With the application of two sorts of theories of elasticity for plates (CPT and FSDT) Malekzadeh et al. [40,41] studied dynamic responses of functionally graded plates under various kinds of moving loads. Şimşek and Aydın [42] studied the dynamic displacement of an imperfect FG plate under a moving load. They examined the influences of some factors including material variation, porosity coefficients and distribution patterns, micro-size parameters and the speed of the moving forces on the transient behaviors. Bi-directional FG rotating heterogeneous cylinders under moving mechanical loads and thermal conditions were fully analyzed by Golzari and Asgari [43]. Recently, Yang et al. [44] scrutinized the time-dependent performances of linearly tapered bi-directional FG beams subjected to a moving harmonic load.

As porosities and micro voids can decrease the strength of structures and due to the significance of design, control, diagnosis and life management of bi-directional functionally graded solids subjected to dynamic forces like moving loads, it is attempted in this study to find ways for improving the structural resistance. Despite using several ways, such as implementing graphene nanoplatelets [45–47], to strengthen mechanical erections, the use of stiffeners can be one of the most effective and affordable methods. They are structural elements with practical significance in applications, namely aircrafts, ships, bridge decks, etc. In this regard, an analysis was performed by Turvey and Der Avanessian [48] to examine the effect of ring-stiffener depth on elastic and elastoplastic large deflection response of steel plates. Some researchers have numerically analyzed different plates connected to eccentrically outside stiffeners with the application of viscos dynamic relaxation method (V-DR). The large deflection of eccentrically stiffened annular functionally graded (FG) sector plates under mechanical and thermo-mechanical loading was obtained by Golmakani and Kadkhodayan [49]. In 2015, Mehrabian and Golmakani [50] dealt with the effects of stiffener depth along with various boundary conditions on static response of annular laminated sector plates. Golmakani and Emami [51] also investigated buckling and large deflection behaviors of radially functionally graded ring-stiffened circular plates based on the DR method. In the case of stiffened shells, Duc and Quan [52] examined the post buckling characteristics of a reinforced double curved shallow shell embedded on elastic mediums in thermal environments according to Galerkin technique and the classical shell theory. Later and on the basis of Reddy's third-order shear deformation shell theory, Duc [53] analyzed the effects of some parameters including the FG power parameters and elastic foundations on thermal dynamic behaviors of stiffened FGM circular cylindrical shells with porosities. A detailed study on nonlinear buckling and post-buckling responses of stiffened functionally graded plates with different geometrical

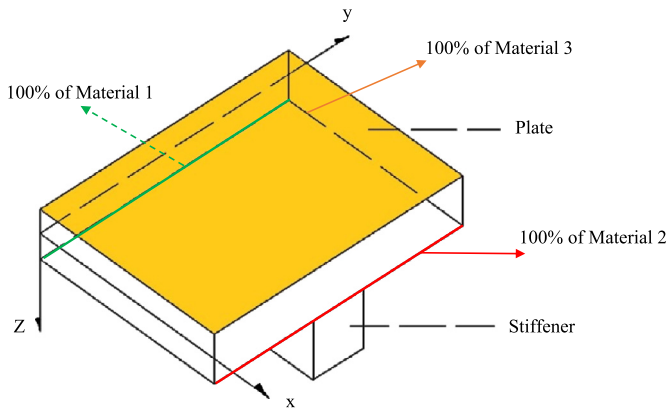

Fig. 1. A schematic of a bi-directional FGM plate with a single stiffener.

properties in thermal environments was prepared by Taczała et al. [54]. Newly, an analytical approach to investigate buckling behaviors of FGM shell segments stiffened by a number of stiffeners in thermal environments was developed by Voung and Duc [55]. There are some other studies performed on stiffened shells with different geometrical shapes [56,57].

To analyze the nonlinear dynamic behaviors of structures, several methods have been proposed. Allahyari et al. [58] used a multiple-scale method to investigate the nonlinear free vibration of a graphene nanoplate. Wang et al. [59] studied the effects of some parameters such as moving velocity and edge constrains on dynamic performances of a moving plate-fluid system by a multiple-scale perturbation technique. Wang et al. [60] also used this method to analyze the nonlinear vibration of FGM sandwich micro cylindrical shells which transport fluid. Another method which can be used to calculate the steady-state response of nonlinear systems is harmonic balance technique. Employing this scheme and Galerkin's method, Wang [61] performed a study on the nonlinear dynamic responses of a composite circular cylindrical shell. There are others numerical methods for obtaining dynamic performances of structures [62–64].

The numerical results of nonlinear dynamic behaviors of eccentrically stiffened rectangular bi-directional functionally graded (2D-FG) plates with micro voids under a moving load with the combination of kinetic dynamic relaxation method (K-DR) and Newmark integration method are presented in this work. Moreover, the effects of different items such as boundary conditions, the material gradient properties (n and m), the porosity volume fraction and the stiffener heights on dynamic characteristics are numerically studied.

2. Theoretical equations

As shown in Fig. 1, a rectangular plate of length a, width b and thickness h is stiffened by a single stiffener of rectangular cross section which is located on the middle of the plate. The plate is assumed to be composed of three distinct constituents whose volume fractions, V_1, V_2 and V_3 change functionally not only from bottom ($z=-h/2$) to top ($z=+h/2$), but also along the x direction [1], Fig. 1. The z and x are the thickness and axial coordinates, respectively. In this section, firstly the effective properties of porous bi-directional FG plates (2D-FG plates) are obtained, and then the dynamic equations of the plates and stiffeners are derived and those of stiffened plates are achieved based on discretely stiffened theory developed by Basu et al. [65].

2.1. Bi-directional FGM plates with porosities

The volume fractions of constituents of the plates can be formulated as bellow [1]:

$$\begin{aligned} V_1 &= \left[1-\left(\frac{z}{h}+\frac{1}{2}\right)^n\right]\left[1-\left(\frac{x}{a}\right)^m\right], \\ V_2 &= \left[1-\left(\frac{z}{h}+\frac{1}{2}\right)^n\right]\left(\frac{x}{a}\right)^m, \\ V_3 &= \left(\frac{z}{h}+\frac{1}{2}\right)^n \end{aligned} \tag{1}$$

where m and n are positive gradient indexes which control the material variation profile in x and z directions, respectively. If $m=0$, the conventional FG plates with two materials (2 and 3) which change functionally through the thicknesses are formed. Once bi-directional FG plates with porosities equally distributed, Fig. 2(a), in all the aforementioned phases are selected, the modified the rule of mixtures can be proposed as Eq. (2),

$$P = P_1\left(V_1-\frac{\alpha_p}{2}\right)+P_2\left(V_2-\frac{\alpha_p}{2}\right)+P_3\left(V_3-\frac{\alpha_p}{2}\right) \tag{2}$$

in which P and α_p are the material properties (Young's modulus, E, Poisson's ratio, ϑ, density, ρ) and porosity fraction, respectively. After substituting Eq. (2) into Eq. (1), Eq. (3) can be improved as

$$\begin{aligned} E(x,z) &= E_1+(E_1-E_2)\left(\frac{z}{h}+\frac{1}{2}\right)^n\left(\frac{x}{a}\right)^m+(E_2-E_1)\left(\frac{x}{a}\right)^m \\ &\quad +(E_3-E_1)\left(\frac{z}{h}+\frac{1}{2}\right)^n-\frac{\alpha_p}{2}(E_1+E_2+E_3) \\ \vartheta(x,z) &= \vartheta_1+(\vartheta_1-\vartheta_2)\left(\frac{z}{h}+\frac{1}{2}\right)^n\left(\frac{x}{a}\right)^m+(\vartheta_2-\vartheta_1)\left(\frac{x}{a}\right)^m \\ &\quad +(\vartheta_3-\vartheta_1)\left(\frac{z}{h}+\frac{1}{2}\right)^n-\frac{\alpha_p}{2}(\vartheta_1+\vartheta_2+\vartheta_3) \\ \rho(x,z) &= \rho_1+(\rho_1-\rho_2)\left(\frac{z}{h}+\frac{1}{2}\right)^n\left(\frac{x}{a}\right)^m+(\rho_2-\rho_1)\left(\frac{x}{a}\right)^m \\ &\quad +(\rho_3-\rho_1)\left(\frac{z}{h}+\frac{1}{2}\right)^n-\frac{\alpha_p}{2}(\rho_1+\rho_2+\rho_3) \end{aligned} \tag{3}$$

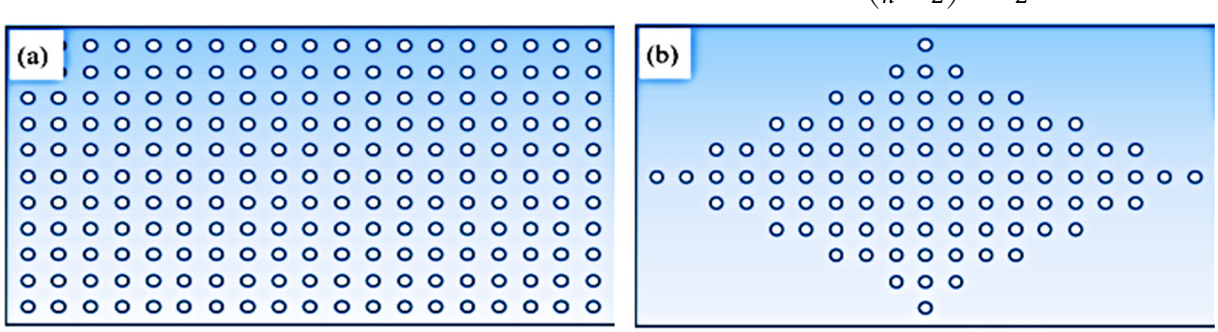

Fig. 2. Porosity configurations in the cross-section areas of porous bi-directional FG plates: (a) even distribution pattern, (b) uneven distribution pattern.

On the other hand, when uneven porosity distribution patterns are considered, Fig. 2(b), the material properties can be obtained by using Eq. (4), Fig. 2(b):

$$\begin{aligned}
E(x,z) &= E_1 + (E_1 - E_2)\left(\frac{z}{h}+\frac{1}{2}\right)^n\left(\frac{x}{a}\right)^m + (E_2 - E_1)\left(\frac{x}{a}\right)^m \\
&\quad + (E_3 - E_1)\left(\frac{z}{h}+\frac{1}{2}\right)^n \\
&\quad - \frac{\alpha_p}{2}(E_1 + E_2 + E_3)\left(1 - \frac{2|z|}{h}\right) \\
\vartheta(x,z) &= \vartheta_1 + (\vartheta_1 - \vartheta_2)\left(\frac{z}{h}+\frac{1}{2}\right)^n\left(\frac{x}{a}\right)^m + (\vartheta_2 - \vartheta_1)\left(\frac{x}{a}\right)^m \\
&\quad + (\vartheta_3 - \vartheta_1)\left(\frac{z}{h}+\frac{1}{2}\right)^n \\
&\quad - \frac{\alpha_p}{2}(\vartheta_1 + \vartheta_2 + \vartheta_3)\left(1 - \frac{2|z|}{h}\right) \\
\rho(x,z) &= \rho_1 + (\rho_1 - \rho_2)\left(\frac{z}{h}+\frac{1}{2}\right)^n\left(\frac{x}{a}\right)^m + (\rho_2 - \rho_1)\left(\frac{x}{a}\right)^m \\
&\quad + (\rho_3 - \rho_1)\left(\frac{z}{h}+\frac{1}{2}\right)^n \\
&\quad - \frac{\alpha_p}{2}(\rho_1 + \rho_2 + \rho_3)\left(1 - \frac{2|z|}{h}\right)
\end{aligned} \tag{4}$$

2.2. Governing plate equations of motion

Fig. 3 illustrates the geometry of a porous 2D-FG rectangular plate carrying a moving line load, q. The origin of Cartesian coordinate is located on the unreformed mid-plane of the plate. Based on the first order shear deformation theory of elasticity, the displacement field is expressed as:

$$\begin{Bmatrix} u_1(x,y,z,t) \\ u_2(x,y,z,t) \\ u_3(x,y,z,t) \end{Bmatrix} = \begin{Bmatrix} u(x,y,t) \\ v(x,y,t) \\ w(x,y,t) \end{Bmatrix} + z \begin{Bmatrix} \psi_x(x,y,t) \\ \psi_y(x,y,t) \\ 0 \end{Bmatrix} \tag{5}$$

where u, v and w are the displacement components of the middle surface in the direction of x, y and z, respectively. Moreover, ψ_x and ψ_y are rotational displacements about the y and x directions, respectively. The general strains can be obtained as:

$$\begin{Bmatrix} \bar{\varepsilon}_{xx} \\ \bar{\varepsilon}_{yy} \\ \bar{\varepsilon}_{xy} \\ \bar{\varepsilon}_{yz} \\ \bar{\varepsilon}_{xz} \end{Bmatrix} = \begin{Bmatrix} \varepsilon_{xx} \\ \varepsilon_{yy} \\ \varepsilon_{xy} \\ \varepsilon_{yz} \\ \varepsilon_{xz} \end{Bmatrix} + z \begin{Bmatrix} \kappa_{xx} \\ \kappa_{yy} \\ \kappa_{xy} \\ \kappa_{yz} \\ \kappa_{xz} \end{Bmatrix} \tag{6}$$

where κ and ε are the components of the curvature and the normal strain. According to the Von-Karman large deflection theory, they can be expressed in the terms of displacements as follows:

$$\begin{Bmatrix} \varepsilon_{xx} \\ \varepsilon_{yy} \\ \varepsilon_{xy} \\ \varepsilon_{yz} \\ \varepsilon_{xz} \end{Bmatrix} = \begin{Bmatrix} u_{,x} + \frac{w_{,x}^2}{2} \\ v_{,y} + \frac{w_{,y}^2}{2} \\ u_{,y} + v_{,x} + w_{,x}w_{,y} \\ \psi_y + w_{,y} \\ \psi_x + w_{,x} \end{Bmatrix} \tag{7}$$

$$\begin{Bmatrix} \kappa_{xx} \\ \kappa_{yy} \\ \kappa_{xy} \\ \kappa_{yz} \\ \kappa_{xz} \end{Bmatrix} = \begin{Bmatrix} \psi_{x,x} \\ \psi_{y,y} \\ \psi_{x,y} + \psi_{y,x} \\ 0 \\ 0 \end{Bmatrix} \tag{8}$$

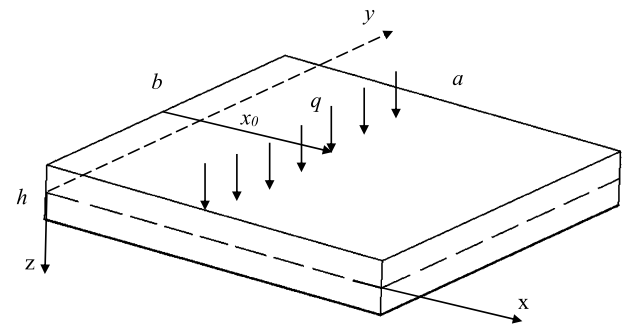

Fig. 3. Geometry and loading of the plate.

Note that the subscript (,) represents the derivative operator with respect to the relevant variable. According to Hook's law, the stress-strain relationships for functionally graded materials can be written as:

$$\begin{Bmatrix} \sigma_{xx} \\ \sigma_{yy} \\ \sigma_{xy} \\ \sigma_{yz} \\ \sigma_{xz} \end{Bmatrix} = \begin{bmatrix} \frac{E(x,z)}{1-\vartheta(x,z)\vartheta(x,z)} & \frac{\vartheta(x,z)E(x,z)}{1-\vartheta(x,z)\vartheta(x,z)} & 0 & 0 & 0 \\ \frac{\vartheta(x,z)E(x,z)}{1-\vartheta(x,z)\vartheta(x,z)} & \frac{E(x,z)}{1-\vartheta(x,z)\vartheta(x,z)} & 0 & 0 & 0 \\ 0 & 0 & G(x,z) & 0 & 0 \\ 0 & 0 & 0 & G(x,z) & 0 \\ 0 & 0 & 0 & 0 & G(x,z) \end{bmatrix} \times \begin{Bmatrix} \bar{\varepsilon}_{xx} \\ \bar{\varepsilon}_{yy} \\ \bar{\varepsilon}_{xy} \\ \bar{\varepsilon}_{yz} \\ \bar{\varepsilon}_{xz} \end{Bmatrix} \tag{9}$$

in which $E(x,z)$, $G(x,z) = E(x,z)/(2(1+\vartheta(x,z)))$ and $\vartheta(x,z)$ are elastic modulus, shear modulus and Poisson's ratio, respectively. To determine the equations of plates, the Hamilton's principle is used:

$$\int_0^T (\delta U + \delta W - \delta K)dt = 0 \tag{10}$$

where K is the virtual kinetic energy of system, U the is strain energy of system and W the is virtual work of external loads. The symbol$\delta$is the variation operator. The resultants stresses are:

$$\begin{aligned}
(N_i, M_i) &= \int_{-\frac{h}{2}}^{\frac{h}{2}} (1,z)\sigma_i dz \quad (i = xx, yy, xy) \\
Q_i &= K^2 \int_{-\frac{h}{2}}^{\frac{h}{2}} \sigma_{iz} dz \quad (i = x, y)
\end{aligned} \tag{11}$$

in which K^2 is the transverse shear correction coefficient equal to 0.833. The moment of inertia is:

$$I_k = \int_{-\frac{h}{2}}^{\frac{h}{2}} \rho(x,z) z^k dz, \quad k = 0, 1, 2 \tag{12}$$

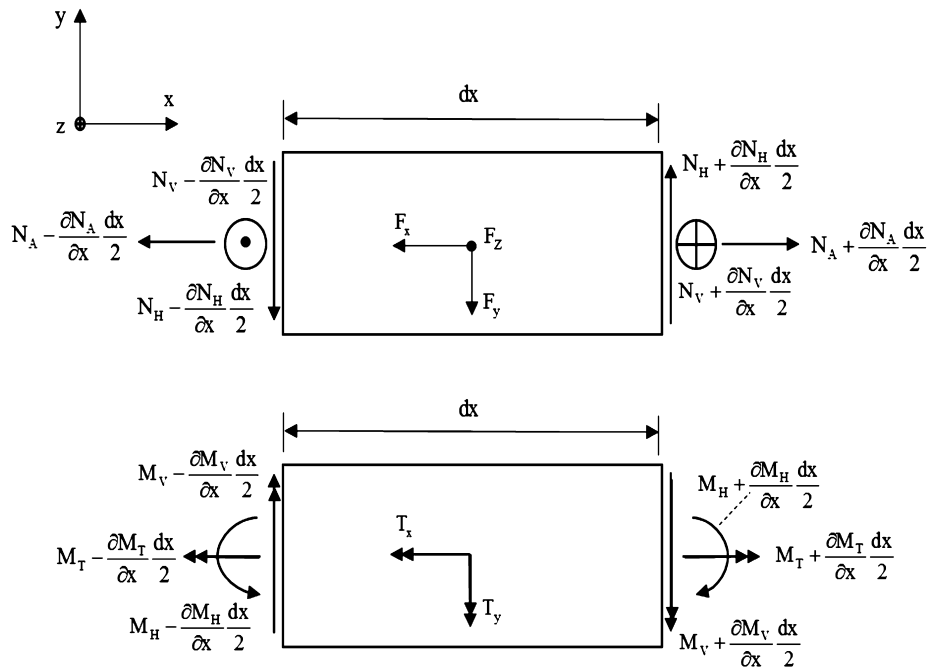

Fig. 4. Forces and moments of a stiffener element.

where $\rho(x, z)$ is the density of the structure. On the basis of FSDT, the dynamic equations of the plate are obtained as [66]:

$$
\begin{aligned}
&N_{xx,x} + N_{xy,y} = I_0\ddot{u} + I_1\ddot{\psi}_x \\
&N_{xy,x} + N_{yy,y} = I_0\ddot{v} + I_1\ddot{\psi}_y \\
&Q_{x,x} + Q_{y,y} + \mathrm{N}(w) + \bar{q} = I_0\ddot{w} \\
&M_{xx,x} + M_{xy,y} - Q_x = I_1\ddot{u} + I_2\ddot{\psi}_x \\
&M_{xy,x} + M_{yy,y} - Q_y = I_1\ddot{v} + I_2\ddot{\psi}_y \\
&\mathbf{N}(w) = N_{xx}w_{,xx} + 2N_{xy}w_{,xy} + N_{yy}w_{,yy}
\end{aligned} \tag{13}
$$

The upper dots denote differential with respect to time. Because of moving load, $\bar{q}(x, y, t)$ is written as:

$$\bar{q}(x, y, t) = q\bar{\delta}(x - x_0) \tag{14}$$

in which q dignifies a moving force and the term $\bar{\delta}$ is the Dirac delta function, integral of which is equal to unity in any neighborhood of $[x_0]$ and zero elsewhere [67].

2.3. Stiffener equations of motion

The field displacement for stiffeners (Eq. (15)) are used for the stiffeners to fully fit those of the plates along the plate-stiffener junction

$$
\begin{Bmatrix} u \\ v \\ w \\ \psi_x \\ \psi_y \end{Bmatrix}^s
=
\begin{bmatrix} 1 & 0 & 0 & e & 0 \\ 0 & 1 & 0 & 0 & e \\ 0 & 0 & 1 & 0 & 0 \\ 0 & 0 & 0 & 1 & 0 \\ 0 & 0 & 0 & 0 & 1 \end{bmatrix}
\begin{Bmatrix} u \\ v \\ w \\ \psi_x \\ \psi_y \end{Bmatrix}^p \tag{15}
$$

Superscripts s and p, represent the stiffener and the plate, respectively, and e $(= [h^s + h^p]/2)$ is the stiffener eccentricity.

The stiffener equilibrium equations are developed by considering the equilibrium between the external interaction forces and moments due to the plate acting on the stiffener and the internal forces and couples acting on a small element of the stiffener [28], Fig. 4. The five equations of motion according to Newton's second law may be written as:

$$
\begin{aligned}
&F_x = N_{A,x} - \rho^s A^s \ddot{u}^s \\
&F_y = M_{H,xx} + N_A v^s_{,xx} + N_{A,x} v^s_{,x} - \rho^s A^s \ddot{v}^s \\
&F_z = N_{V,x} + N_A w^s_{,xx} + N_{A,x} w^s_{,x} - \rho^s A^s \ddot{w}^s \\
&T_y = -N_V + M_{V,x} + e(N_{A,x}) + M_{T,y} - \frac{1}{12}\rho^s A^s \left(h^s\right)^2 \ddot{\psi}^s_x \\
&T_x = M_{T,x} - I^s_p \ddot{\psi}^s_y
\end{aligned} \tag{16}
$$

where N_A denotes the axial force of the stiffener and N_V is the shear force perpendicular to the central axis of the stiffener cross-section. M_T, M_V, M_H also indicate the torque and moments about the x, y, z axes, respectively, through the centroid of the stiffener cross-section. As previously mentioned, e denotes the vertical distance of center area of stiffener from the mid-plane of the plate and I^s_p is the polar mass moment of inertia.

The forces, bending and torsion moments of the stiffener may be calculated as:

$$
\begin{aligned}
&N_A = E^s b^s h^s \varepsilon^s_{xx} \\
&N_V = K^2 G^s \varepsilon^s_{xz} \\
&M_V = \frac{E^s (h^s)^3 b^s}{12}\left(\kappa^s_{xx}\right) \\
&M_T = K^s G^s h^s \left(b^s\right)^3 \left(\kappa^s_{xy}\right)
\end{aligned} \tag{17}
$$

where b^s, h^s, E^s and G^s are the width, depth, Young and shear moduli of the stiffener, respectively and K^s is a numerical factor which depends on the ratio of b^s/h^s [28]. It is noted that the stiffener is modeled as a beam and placed along plate nodal lines. For a stiffener (beam) bending moment, M_H is zero [68].

As stated for the plate, the components of the curvature and normal strain for the stiffener can be expressed in terms of the displacements as:

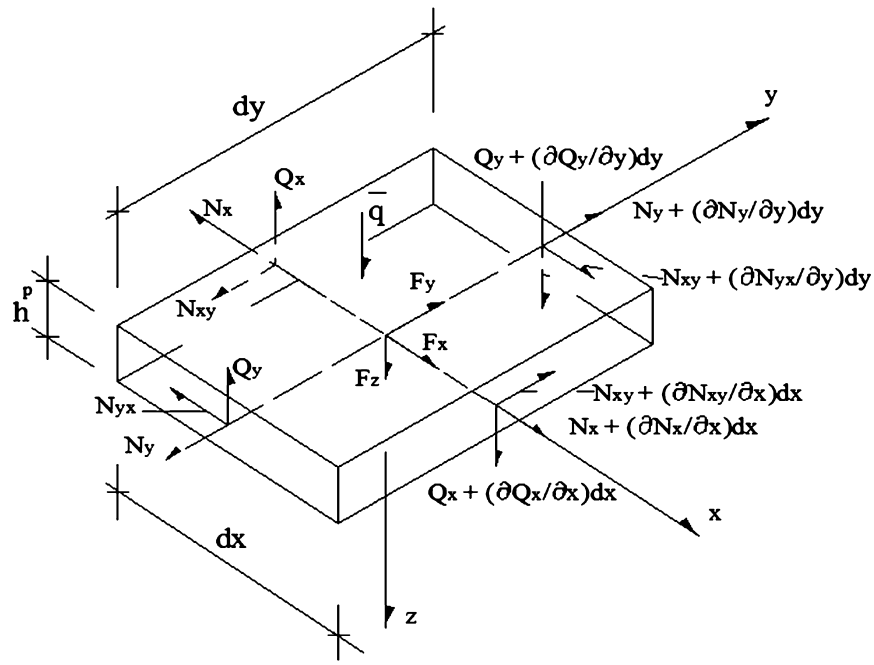

Fig. 5. Forces in a deformed element of a stiffened plate.

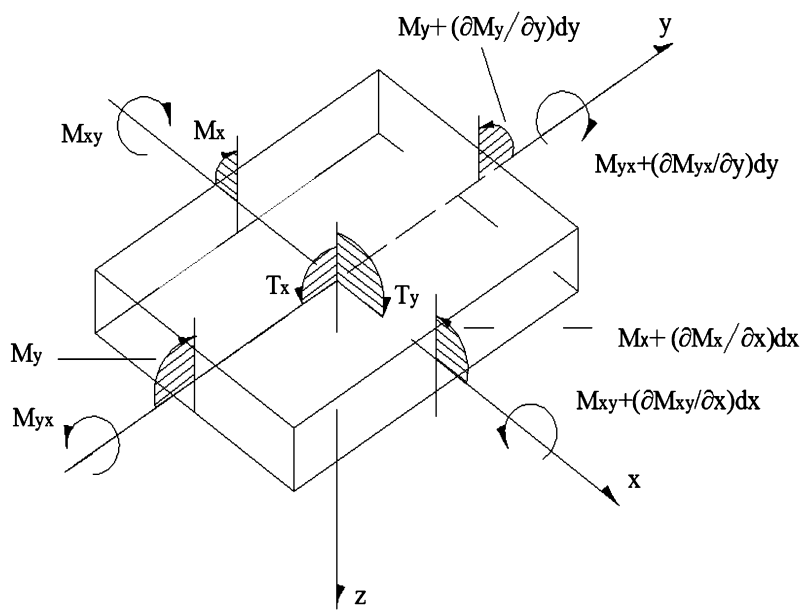

Fig. 6. Moments in a deformed element of a stiffened plate.

$$\varepsilon^s_{xx} = u^s_{,x} + \left(\frac{w^s}{2}\right)^2 + \left(\frac{v^s}{2}\right)^2$$
$$\varepsilon^s_{xz} = \psi^s_x + w^s_{,x}$$
$$\kappa^s_{xx} = \psi^s_{x,x}$$
$$\kappa^s_{xy} = \psi^s_{x,y} + \psi^s_{y,x} \tag{18}$$

2.4. Governing stiffened plate equations of motion

Applying the dynamic equations of plates and stiffeners from sections 2.2 and 2.3, the stiffened plate equations of motion can be achieved. The stiffened plate can be considered as a typical plate which is subjected to the reaction forces of the stiffener. The forces and moments acting on an element of a stiffened rectangular plate are shown in Figs. 5 and 6. By defining quantity Δy as the width of plate over which the surface forces are assumed to be distributed, the equations of motion based on FSDT take that following forms:

$$N_{xx,x} + N_{xy,y} + \frac{F_x}{\Delta y} = I_0\ddot{u} + I_1\ddot{\psi}_x$$
$$N_{xy,x} + N_{yy,y} + \frac{F_y}{\Delta y} = I_0\ddot{v} + I_1\ddot{\psi}_y$$
$$Q_{x,x} + Q_{y,y} + \mathrm{N}(w) + \bar{q} + \frac{F_z}{\Delta y} = I_0\ddot{w}$$
$$M_{xx,x} + M_{xy,y} - Q_x + \frac{T_y}{\Delta y} = I_1\ddot{u} + I_2\ddot{\psi}_x$$
$$M_{xy,x} + M_{yy,y} - Q_y + \frac{T_x}{\Delta y} = I_1\ddot{v} + I_2\ddot{\psi}_y \tag{19}$$

in which

$$\mathbf{N}(w) = N_{xx}w_{,xx} + 2N_{xy}w_{,xy} + N_{yy}w_{,yy} \tag{20}$$

2.5. The stiffened plate boundary conditions

The boundary conditions used in present study are presented as follows:

a) *For simply supported boundary condition* (*SSSS*):

$$\begin{cases} x=0, & a \to u=v=w=\psi_y=M_x=0 \\ y=0, & b \to u=v=w=\psi_x=M_y=0 \end{cases} \tag{21}$$

b) *For clamped boundary condition* (*CCCC*):

$$\begin{cases} x=0, & a \to u=v=w=\psi_x=\psi_y=0 \\ y=0, & b \to u=v=w=\psi_x=\psi_y=0 \end{cases} \tag{22}$$

c) *For SCSC* (*parallel edges are in the same conditions*):

$$\begin{cases} x=0, & a \to u=v=w=\psi_y=M_x=0 \\ y=0, & b \to u=v=w=\psi_x=\psi_y=0 \end{cases} \tag{23}$$

d) *For SCCC*:

$$\begin{cases} x=0 \to u=v=w=\psi_y=M_x=0 \\ x=b, \quad y=0, \quad b \to u=v=w=\psi_x=\psi_y=0 \end{cases} \tag{24}$$

As mentioned earlier, the displacements vectors of the stiffener are obtained by the plate displacements, so that the plate boundary conditions can satisfy the equations of the stiffener.

3. Solution methodology of the nonlinear equations

In this section, the kinetic dynamic relaxation method modified along with Newmark integration which can solve the nonlinear dynamic differential equations is proposed. In the following, the Newmark integration and the K-DR method are explained. Then, the algorithm of modified kinetic dynamic relaxation method is presented.

3.1. Newmark integration method

According to Newmark method, the first and the second derivatives of the nodal displacements, $\boldsymbol{x} = \boldsymbol{u}, \boldsymbol{v}, \boldsymbol{w}, \boldsymbol{\psi}_x, \boldsymbol{\psi}_y$, at t_{j+1} ($j =$ the number of time steps) can be computed as:

$$\ddot{\boldsymbol{x}}_{\boldsymbol{j}+1} = \left(\frac{1}{\beta(\Delta t_j)^2}\Delta\boldsymbol{x}_{\boldsymbol{j}} - \frac{1}{\beta\Delta t_j}\dot{\boldsymbol{x}}_{\boldsymbol{j}} - \left(\frac{1}{2\beta}-1\right)\ddot{\boldsymbol{x}}_{\boldsymbol{j}}\right) \tag{25}$$

$$\dot{\boldsymbol{x}}_{\boldsymbol{j}+1} = \left(\frac{\gamma}{\beta\Delta t_j}\Delta\boldsymbol{x}_{\boldsymbol{j}} - \left(\frac{\gamma}{\beta}-1\right)\dot{\boldsymbol{x}}_{\boldsymbol{j}} - \left(\frac{\gamma}{2\beta}-1\right)\Delta t_j\ddot{\boldsymbol{x}}_{\boldsymbol{j}}\right) \tag{26}$$

in which β and γ are Newmark constants which control the stability and accuracy of the response. To obtain stable and convergent results, for pulse distributed loads $\gamma = 0.5$ and $\beta = 0.25$ (constant average acceleration method) and for moving loads $\gamma = 1.5$ and $\beta = 0.8$ (Galerkin method) are used and Δt shows the time interval.

By substituting Eq. (25) into Eq. (19), the equivalent static form is achieved as:

$$\begin{aligned} &N_{xx,x} + N_{xy,y} + \frac{F_x}{\Delta y} - A_0(I_0\boldsymbol{u}_{j+1} + I_1\boldsymbol{\psi}_{x_{j+1}}) \\ &= -\big\{I_0[A_0\boldsymbol{u}_j + A_1\dot{\boldsymbol{u}}_j + A_2\ddot{\boldsymbol{u}}_j] \\ &\quad + I_1[A_0\boldsymbol{\psi}_{x_j} + A_1\dot{\boldsymbol{\psi}}_{x_j} + A_2\ddot{\boldsymbol{\psi}}_{x_j}]\big\} \\ &N_{xy,x} + N_{yy,y} + \frac{F_y}{\Delta y} - A_0(I_0\boldsymbol{v}_{j+1} + I_1\boldsymbol{\psi}_{y_{j+1}}) \\ &= -\big\{I_0[A_0\boldsymbol{v}_j + A_1\dot{\boldsymbol{v}}_j + A_2\ddot{\boldsymbol{v}}_j] \\ &\quad + I_1[A_0\boldsymbol{\psi}_{y_j} + A_1\dot{\boldsymbol{\psi}}_{y_j} + A_2\ddot{\boldsymbol{\psi}}_{y_j}]\big\} \\ &Q_{x,x} + Q_{y,y} + \mathbf{N}(w) + \frac{F_z}{\Delta y} - A_0I_0\boldsymbol{w}_{j+1} \\ &= -I_0[A_0\boldsymbol{w}_j + A_1\dot{\boldsymbol{w}}_j + A_2\ddot{\boldsymbol{w}}_j] - \bar{q}(x,y,t) \\ &M_{xx,x} + M_{xy,y} - Q_x + \frac{T_y}{\Delta y} - A_0(I_1\boldsymbol{u}_{j+1} + I_2\boldsymbol{\psi}_{x_{j+1}}) \\ &= -\big\{I_1[A_0\boldsymbol{u}_j + A_1\dot{\boldsymbol{u}}_j + A_2\ddot{\boldsymbol{u}}_j] \\ &\quad + I_2[A_0\boldsymbol{\psi}_{x_j} + A_1\dot{\boldsymbol{\psi}}_{x_j} + A_2\ddot{\boldsymbol{\psi}}_{x_j}]\big\} \\ &M_{xy,x} + M_{yy,y} - Q_y + \frac{T_x}{\Delta y} - A_0(I_1\boldsymbol{v}_{j+1} + I_2\boldsymbol{\psi}_{y_{j+1}}) \\ &= -\big\{I_1[A_0\boldsymbol{v}_j + A_1\dot{\boldsymbol{v}}_j + A_2\ddot{\boldsymbol{v}}_j] \\ &\quad + I_2[A_0\boldsymbol{\psi}_{y_j} + A_1\dot{\boldsymbol{\psi}}_{y_j} + A_2\ddot{\boldsymbol{\psi}}_{y_j}]\big\} \end{aligned} \tag{27}$$

where

$$A_0 = \frac{1}{\beta(\Delta t_j)^2}, \qquad A_1 = \frac{1}{\beta\Delta t_j}, \qquad A_2 = \frac{1}{2\beta} - 1 \tag{28}$$

A briefed form of Eq. (27) can be written as below:

$$[\bar{\boldsymbol{K}}_{j+1}]\boldsymbol{x}_{j+1} = \{\bar{\boldsymbol{P}}_{j+1}\} \tag{29}$$

where $[\bar{\boldsymbol{K}}_{j+1}]$ and $\{\bar{\boldsymbol{P}}_{j+1}\}$ are the equivalent stiffness matrix (the left-hand side of Eq. (27)) and equivalent load vector (the right-hand side of Eq. (27)), respectively.

3.2. Dynamic relaxation method with kinetic damping

To solve the dynamic equations Newmark's method has to be combined with a numerical technique. In this study, for the sake of simplicity, efficiency and unique procedure for both linear and nonlinear systems, the dynamic relaxation method is adopted. According to this method and based on the viscos damping (V-DR) the equivalent static system has to be transferred to an artificial dynamic space by adding artificial mass and damping terms [39] as:

$$[\boldsymbol{M}]^n_{DR}\{\boldsymbol{a}\}^n + [\boldsymbol{C}]^n_{DR}\{\boldsymbol{v}\}^n + [\bar{\boldsymbol{K}}_{\boldsymbol{j}+1}]^{\boldsymbol{n}}\boldsymbol{x}^n_{j+1} = \bar{\boldsymbol{P}}^n_{j+1} \tag{30}$$

Here, $[\boldsymbol{M}]^n_{DR}$ and $[\boldsymbol{C}]^n_{DR}$ are diagonal fictitious mass and damping matrices in nth iteration of DR, respectively [70]. Moreover, $\{\boldsymbol{v}\}$ and $\{\boldsymbol{a}\}$ are fictitious velocity and acceleration vectors. On the other hand, in the use of kinetic dynamic relaxation method, the determination of fictitious damping term is not required and Eq. (30) can be reformed as below:

$$[\boldsymbol{M}]^n_{DR}\{\boldsymbol{a}\}^n + [\bar{\boldsymbol{K}}_{j+1}]^{\boldsymbol{n}}\boldsymbol{x}^n_{j+1} = \bar{\boldsymbol{P}}^n_{j+1} \tag{31}$$

Similar to the viscos DR formulation [69,70], the kinetic DR technique uses the central finite differences to integrate the fictitious equations of motion which provides the following fundamental relationships:

$$\{\boldsymbol{v}\}^{\boldsymbol{n}+1/2} = \boldsymbol{v}^{\boldsymbol{n}-1/2} + \frac{\tau^n}{[\boldsymbol{M}]_{\boldsymbol{DR}}}\{\boldsymbol{R}\}^{\boldsymbol{n}} \tag{32}$$

$$\{\boldsymbol{x}\}^{\boldsymbol{n}+1} = \{\boldsymbol{x}\}^{\boldsymbol{n}} + \tau^n\{\boldsymbol{v}\}^{\boldsymbol{n}+\frac{1}{2}} \tag{33}$$

Here, symbol τ^n indicates the fictitious time step in nth DR iteration and is usually taken equal to 1 to guarantee convergence of the K-DR method and $\{\boldsymbol{R}\}^n$ is residual force vector obtained as:

$$\{\boldsymbol{R}^n\} = \bar{\boldsymbol{P}}^n_{j+1} - [\bar{\boldsymbol{K}}_{j+1}]^{\boldsymbol{n}}\boldsymbol{x}^n_{j+1} \tag{34}$$

The kinetic energy of the whole system is calculated by following equation:

$$KE^{n+1} = \frac{1}{2}\sum_{i=1}^{N} \boldsymbol{m}_{ii}^{\mathbf{n}} \left(v_i^{\mathbf{n}+\frac{1}{2}}\right)^2 \tag{35}$$

in which, N represents the number of degrees of freedom. By comparison the current kinetic energy with the previous one, the peak of kinetic energy can be achieved. When the peak is detected, all current nodal velocities are set to zero and then a new iteration of K-DR restarted with the initial nodal displacement proposed by Topping and Ivanyi [71] as follows:

$$\{\boldsymbol{x}\}^{n-1/2} = \{\boldsymbol{x}\}^n - \left(\frac{3}{2}\tau^n\right)\{\boldsymbol{v}\}^{n+\frac{1}{2}} + \frac{(\tau^n)^2}{2(\boldsymbol{m}_{DR})_{ii}^n} + \left\{\boldsymbol{R}^n\right\} \tag{36}$$

The nodal velocity at the first-time step can be obtained as [72]:

$$\{\boldsymbol{v}\}^{n+\frac{1}{2}} = \frac{\tau^n}{2(\boldsymbol{m}_{DR})_{\boldsymbol{ii}}^{\boldsymbol{n}}}\{\boldsymbol{R}\}^{\boldsymbol{n}} \tag{37}$$

This sequential procedure is continued until the appropriate convergence criterion are satisfied.

As mentioned before, K-DR method is achieved only by adding the artificial mass term to a static equation. To guarantee the numerical convergence in K-DR method, the fictitious mass matrix elements are calculated in accordance with Gershgörin theorem [73]:

$$\boldsymbol{m}_{ii}^l \geq \frac{1}{2}\left(\tau^n\right)^2 \sum_{j=1}^{N} \left|k_{ij}^l\right|, \quad \boldsymbol{k} = \frac{\partial\{[\bar{\boldsymbol{K}}]^n x^n\}}{\partial x} \tag{38}$$

where superscript l represents $\boldsymbol{u}, \boldsymbol{v}, \boldsymbol{w}, \boldsymbol{\psi}_x, \boldsymbol{\psi}_y$. In the following part, the modified kinetic dynamic relaxation algorithm is provided. The steps are repeated until dynamic analysis time is complete. It should be noted that there are two convergence criteria to stop the iterations of K-DR, namely, disequilibrium (residual) force and kinetic energy of the system.

1. *Specify the number of time step* (NT).
2. *Set initial artificial velocity, initial displacement* (*converged displacement at previous time step*) *and the number of maximum iteration* ($n_{\max}$).
3. *Construct artificial diagonal mass matrix using Eq.* (38).
4. *Calculate disequilibrium force* $\{\boldsymbol{R}\}^n$.
5. *If* $|\boldsymbol{r}_i^n| \approx 0$, *go to* (12), *otherwise, continue.*
6. *Calculate* $\{\boldsymbol{v}\}^{n+1/2}$ *using Eq.* (37).
7. *If* $\sum_{i=1}^{N} \boldsymbol{m}_{ii}^n (\boldsymbol{v}_i^{n+1/2})^2 \approx 0$, *go to* (12), *otherwise, continue.*
8. *Calculate the kinetic energy by Eq.* (35).
9. *If* $KE^{(n+1)} < KE^n$, *calculate the displacement and velocity vectors using Eqs.* (36) *and* (37) *then go to* (3), *otherwise, continue.*
10. *Calculate* $\{\boldsymbol{x}\}^{n+1}$ *using Eq.* (33).
11. $n = n + 1$, *if* $(n < n_{\max})$ *go to* (3), *otherwise, continue.*
12. *Calculate* $\{\dot{\boldsymbol{x}}\}$ *and* $\{\ddot{\boldsymbol{x}}\}$ *using* (*Eqs.* (25) *and* (26)).
13. $j = j + 1$, *if* $(j < NT)$ *go to* (2), *otherwise, print results.*

The above algorithm demonstrates that the kinetic dynamic relaxation method can be combined with an implicit integration method easily.

4. Numerical results and discussions

In this section, different case studies are investigated for static/dynamic analysis of rectangular plates with/without stiffeners subjected to different loads and boundary conditions to illustrate firstly the efficiency and accuracy of the present analysis and secondly the stiffener effect on the central deflection of 2D-FG plates with two porosity distribution patterns (even and uneven).

Table 1
Comparison of maximum deflections of K-DR with those of V-DR and Abaqus finite element for a square plate in diverse boundary conditions.

B.Cs	Method	Deflection (mm)	Iteration
SSSS	Viscos damping	6.60	634
	Kinetic damping	6.60	374
	Abaqus	6.65	–
CCCC	Viscos damping	5.6463	625
	Kinetic damping	5.6495	394
	Abaqus	5.54	–

4.1. Comparison study

Case study 1. In this case, kinetic DR (K-DR) results for the large deflection bending analysis of a rectangular plate in fully simply supported and clamped boundary conditions under a static uniform load of $\bar{q} = 50$ MPa are compared with the results obtained by the viscos DR (V-DR) and Abaqus finite element. Properties and dimensions of plate are as (Eq. (39)):

$$\begin{aligned} &a = b = 0.12 \text{ m} \quad h = 0.004 \text{ m} \\ &E = 200 \text{ GPa} \qquad \vartheta = 0.3 \end{aligned} \tag{39}$$

Table 1 shows a comparison between the results obtained by K-DR and V-DR and finite element methods. In addition to the accuracy, it is seen that compared to V-DR, the K-DR has a faster convergence rate with fewer iterations.

Case study 2. In the second case, to verify the present results for nonlinear dynamic analysis, the obtained results of a fully clamped square FG plate ($a = b = 1$) with thickness-to-length ratio (h/a) of 0.2 under a time harmonic load are compared with those reported by Mojdehi et al. [74]. Also, it is assumed that material properties of the plate vary functionally from bottom (1) to top (2) and dimensionless central deflection and axial stress can be obtained as:

$$\begin{aligned} &W = \frac{100E_1h^3w}{12a^4(1-\nu_1^2)q_0} \\ &\Theta = \frac{h^2}{q_0a^2}\sigma_{xx} \end{aligned} \tag{40}$$

in which q_0 is a distributed load and equal to 1 MPa. The presumed properties, dimensions and load are as:

$$\begin{aligned} &E_1 = 70 \text{ GPa}, \qquad \rho_1 = 2702\ \frac{\text{kg}}{\text{m}^3}, \qquad \vartheta_1 = 0.3 \\ &E_2 = 200 \text{ GPa}, \qquad \rho_2 = 5700\ \frac{\text{kg}}{\text{m}^3}, \qquad \vartheta_2 = 0.3 \\ &\bar{q}(x, y, t) = q_0 \sin(2000t) \end{aligned} \tag{41}$$

As illustrated in Figs. 7 and 8, the obtained results are in good consistency with those given in [74].

Case study 3. The effects of linear and nonlinear systems on the frequency of structures are shown in Fig. 9. To do this, a square plate under the dynamic pressure forces with graded materials from lower (1) to upper surface (2) and following parameters are examined.

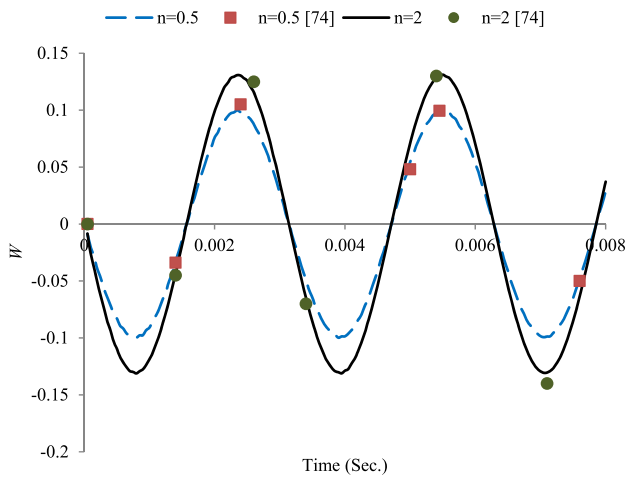

Fig. 7. Time history of the non-dimensional centroidal deflection of a fully clamped square FG plate.

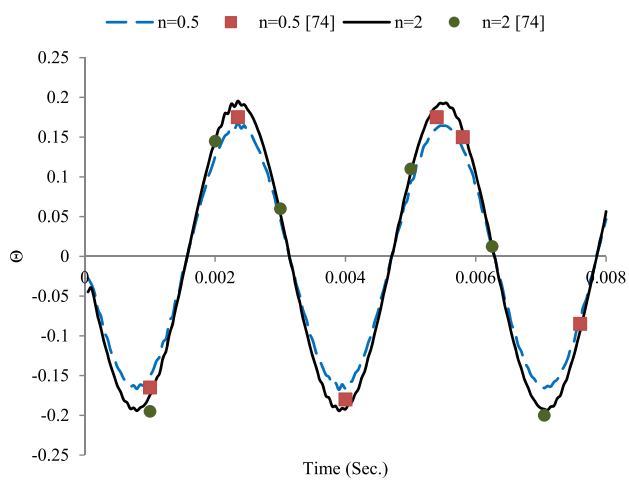

Fig. 8. Time history of the non-dimensional axial stress at the centroid of the top surface of a fully clamped square FG plate.

$$a = b = 1 \text{ m}, \qquad h = 0.05 \text{ m}$$
$$\text{ZrO}_2\text{: } E_1 = 200 \text{ GPa}, \qquad \rho_1 = 7850 \frac{\text{kg}}{\text{m}^3}, \qquad \vartheta_1 = 0.3$$
$$\text{Sic: } E_2 = 380 \text{ GPa}, \qquad \rho_2 = 3960 \frac{\text{kg}}{\text{m}^3}, \qquad \vartheta_2 = 0.18 \tag{42}$$

Fig. 9 provides information on the central displacements (w/h) of a SSSS FGM plate with $n = 5$ and $\alpha_p = 0.2$ versus time for different amplitudes of applied forces. According to Fig. 9, it is observed that the magnitudes of vertical displacement witness noticeable increases with the rise of load values. Moreover, in a linear system, frequency magnitude of 0.87 (Hz) has no change for every load value, while when it comes to a nonlinear theory, it increases by growing load amplitudes.

Case study 4. In this case, the validity of the present numerical method for the dynamic (transient) analysis of rectangular plates carrying moving dynamic loads is examined. To do this, the results obtained by K-DR for clamped and simply supported boundary conditions are compared with those obtained by Eftekhari [75]. The parameters used here are as follows:

$$\frac{\rho h}{D} = 1, \qquad \frac{q}{D} = 1, \qquad a = b = 1,$$
$$x_0 = vt, \qquad y_0 = \frac{1}{2} \tag{43}$$

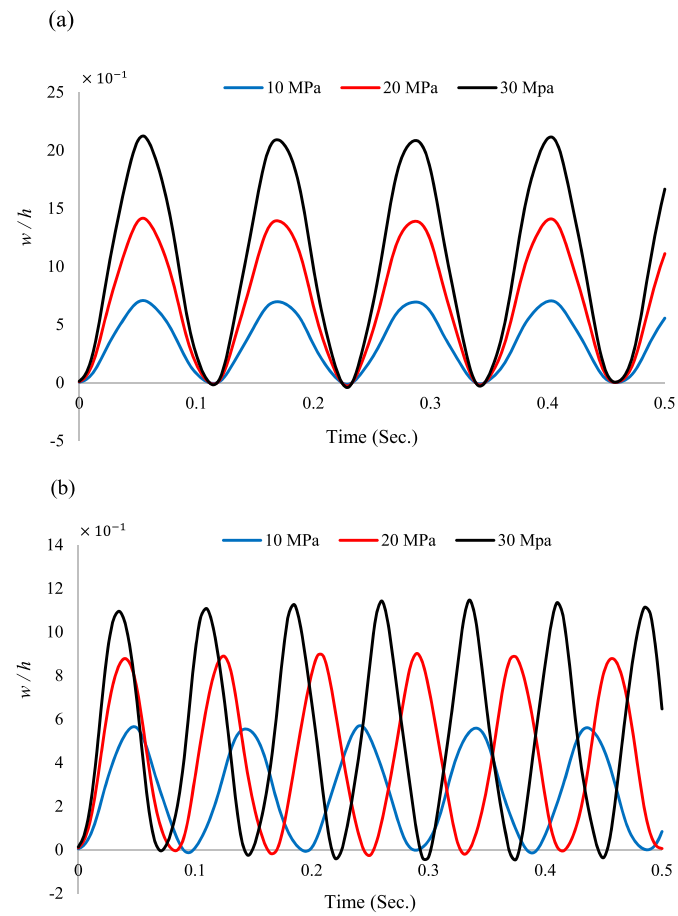

Fig. 9. Effects of load increments on the value of w/h: (a) linear theory, (b) nonlinear theory, $\alpha_p = 0.2$.

Table 2
Comparison of obtained central static deflection on the basis of FSDT and CPT with Abaqus (SSSS).

Depth ratio (Ω)	CPT	FSDT	Abaqus
0	6.60	6.61	6.65
1.5	5.64	5.64	5.70
3	3.32	3.88	3.89

in which v is the velocity of the moving load in the x-direction, t is the time required for the load q to traverse the plate, D is the flexural rigidity and y_0 is the normal distance from the x axis. Figs. 10 and 11 demonstrate the accuracy of K-DR method for CCCC and SSSS boundary conditions, respectively.

Case study 5. Here, the numerical results based on classic plate theory (CPT) and first order shear deformation theory (FSDT), are compared to each other. The equations of stiffeners are also obtained by using these two theories. The dimensions and mechanical properties of the SSSS plate and stiffener are similar in the case study 1. Table 2 provides comparison of results obtained by FSDT and CPT with those of Abaqus. As expected, as depth ratio $\Omega = h^s/h$ becomes larger, FSDT results will become more accurate than those obtained through CPT.

Case study 6. The central dynamic (transient) responses of a stiffened rectangular plate in simply supported boundary condition subjected to a uniform mechanical load are compared with those of Abaqus finite element in Fig. 12. The taken parameters are:

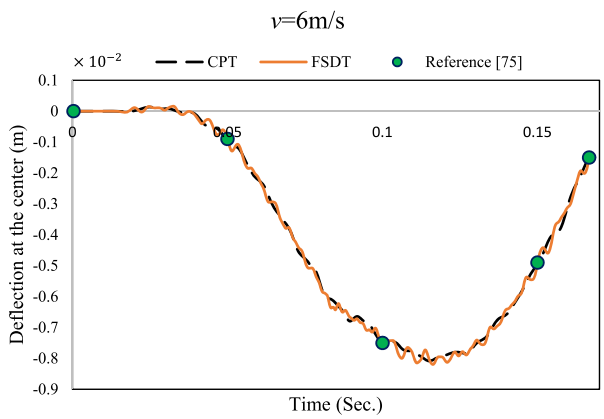

Fig. 10. Comparison of numerical results for central deflection of a fully clamped square plate subjected to a moving load.

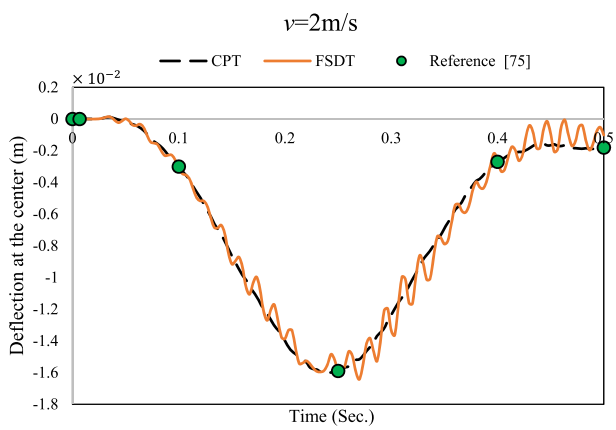

Fig. 11. Comparison of numerical results for central deflection of a fully simply supported square plate subjected to a moving load.

$$a = b = 0.3 \text{ m}, \qquad h = 0.03 \text{ m}$$
$$E = E^s = 21 \times 10^9 \ \frac{\text{N}}{\text{m}^2}, \qquad \vartheta = \vartheta^s = 0.25$$
$$\rho = \rho^s = 800 \text{ N}.\frac{\text{s}^2}{\text{m}^4},$$
$$\bar{q}(x, y, t) = 50000 \ \frac{\text{N}}{\text{m}^2} \quad 0 \le t \le \infty \tag{44}$$

As mentioned before, superscript s denotes stiffener. Moreover, the ratios of stiffener depth to the thickness of the plate and stiffener width to its depth are $\Omega = h^s/h = 1$ and $b^s/h^s = 1$, respectively. It can be observed that the current results are in good agreement with those of Abaqus.

4.2. Parametric study

In what follows, the numerical results of a square-shaped porous FG plate of side equal to 1 m ($a = b = 1$ m) and the ratio of its thickness to length as 0.1, stiffened by one stiffener under a moving line load q, with different velocities and boundary conditions are presented. The porous 2D-FG plate is formed of aluminum (Al), zirconia (ZrO_2) and a ceramic (Sic) with the following material properties as:

$$AL\text{: } E_1 = 70 \text{ GPa}, \qquad \rho_1 = 2702 \ \frac{\text{kg}}{\text{m}^3}, \qquad \vartheta_1 = 0.3$$
$$ZrO_2\text{: } E_2 = 200 \text{ GPa}, \qquad \rho_2 = 7850 \ \frac{\text{kg}}{\text{m}^3}, \qquad \vartheta_2 = 0.3$$
$$\text{Sic: } E_3 = 380 \text{ GPa}, \qquad \rho_3 = 3960 \ \frac{\text{kg}}{\text{m}^3}, \qquad \vartheta_3 = 0.18 \tag{45}$$

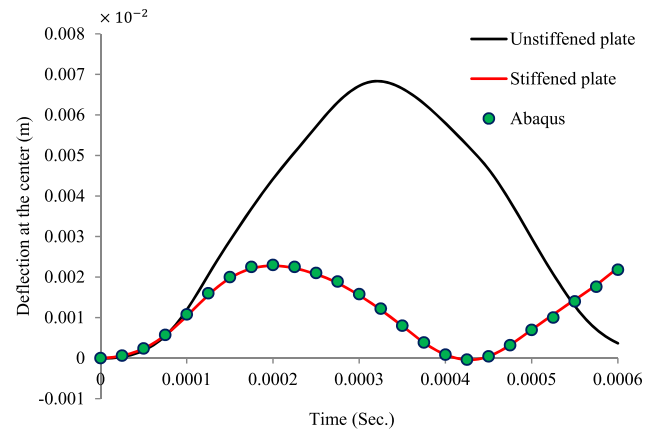

Fig. 12. Transient central deflection of a simply supported stiffened rectangular plate.

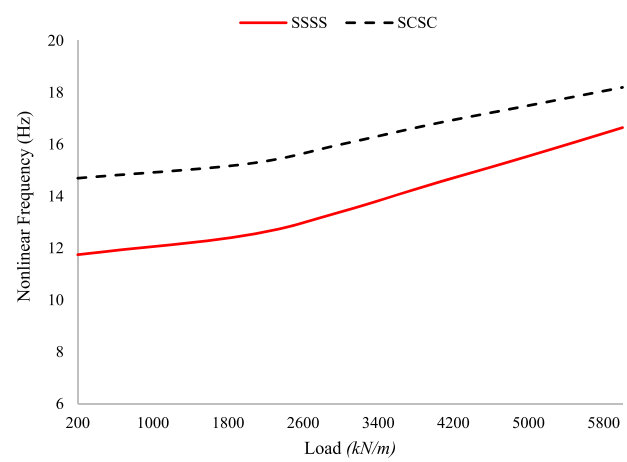

Fig. 13. Nonlinear frequencies of the porous bi-directional functionally graded plates for different load amplitudes and boundary conditions ($n = m = 4$ and $\alpha_p = 0.1$).

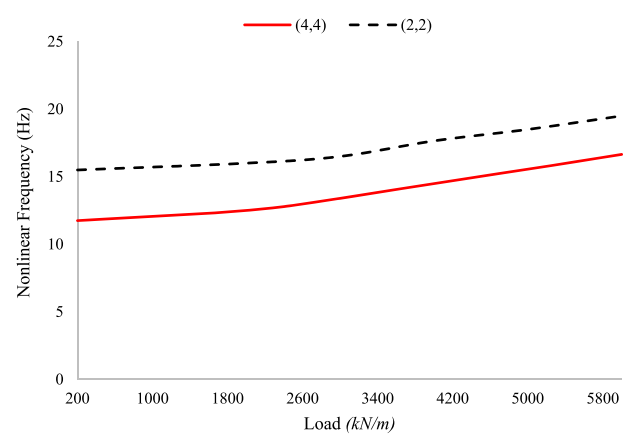

Fig. 14. Nonlinear frequencies of the porous bi-directional functionally graded plates for different load amplitudes and FG indices (n, m). ($\alpha_p = 0.1$).

and the load, which moves in the axial direction of the plate with constant velocity, v, is taken as:

$$q = 400 \ \frac{\text{kN}}{\text{m}}, \qquad x_0 = vt \tag{46}$$

Furthermore, the width of rectangular cross section stiffener is equal to plate thickness and this isotropic stiffener has the same mechanical properties as material 2 (ZrO_2).

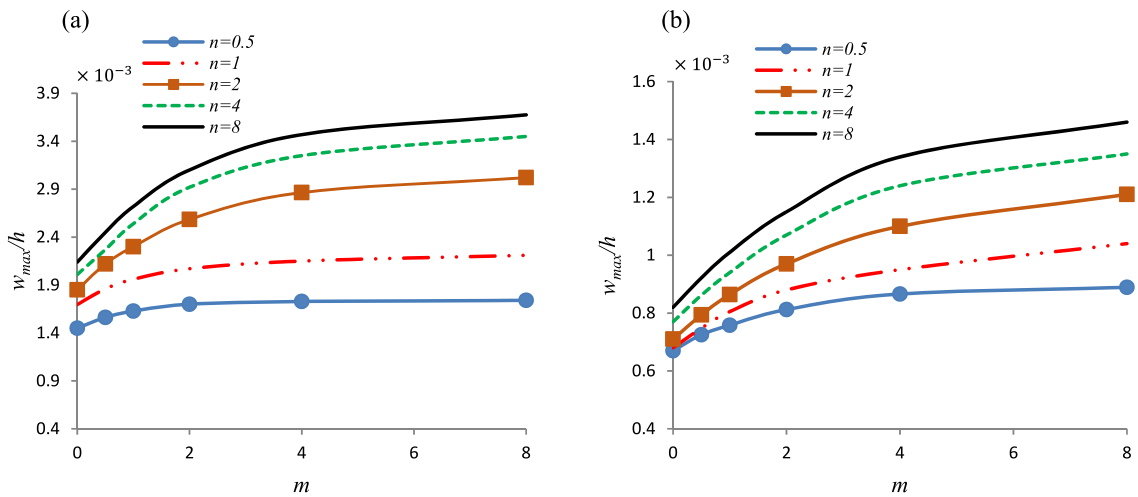

Fig. 15. Effects of gradient indexes (n, m) on the value of $w_{\max}/h$. (a) SSSS, (b) CCCC.

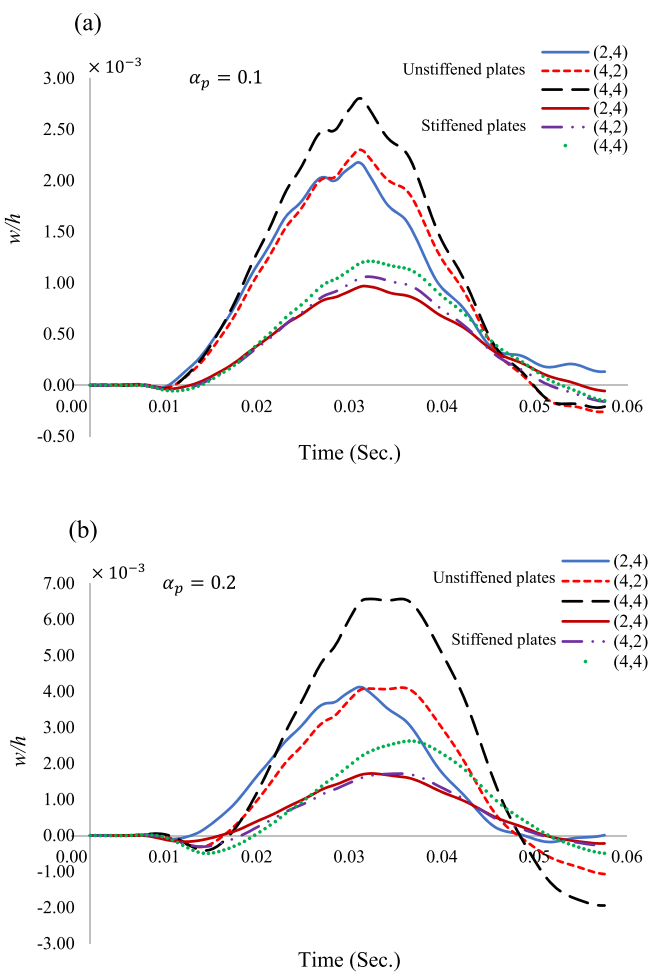

Fig. 16. Dimensionless deflections at the center of the unstiffened/stiffened 2D-FG plate with evenly distributed porosities under a moving load in SCSC boundary condition. (a) $\alpha_p = 0.1$, (b) $\alpha_p = 0.2$.

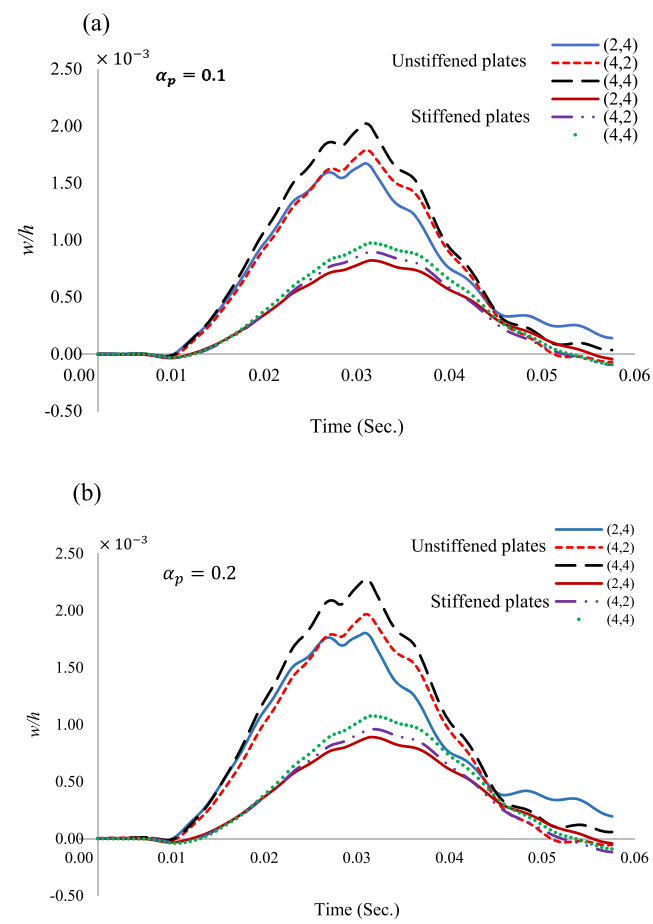

Fig. 17. Dimensionless deflections at the center of the unstiffened/stiffened 2D-FG plate with unevenly distributed porosities under a moving load in SCSC boundary condition. (a) $\alpha_p = 0.1$, (b) $\alpha_p = 0.2$.

Fig. 13 illustrates the variation of nonlinear frequencies (v/a) versus dynamic loads for the even distribution $(\alpha_p = 0.1)$ for SSSS and SCSC conditions when $(n, m) = (4, 4)$. For both types of edge conditions, there is a direct relationship between the nonlinear frequencies and the magnitudes of applied loads in a such way that the more force values are exerted, the more frequencies is observed. However, the impact of loads on the SSSS plate's frequency is fairly more than that of the SCSC plate.

The comparison of the nonlinear frequency between two simply supported 2D-FGM plates ($n = m = 2$ and $n = m = 4$) with an even porosity distribution $(\alpha_p = 0.1)$ is presented in Fig. 14. It is seen that the nonlinear frequencies of the 2D-FGM plates decrease with an increase in amount of n and m because the behavior of 2D-FGM plates tends to ductility.

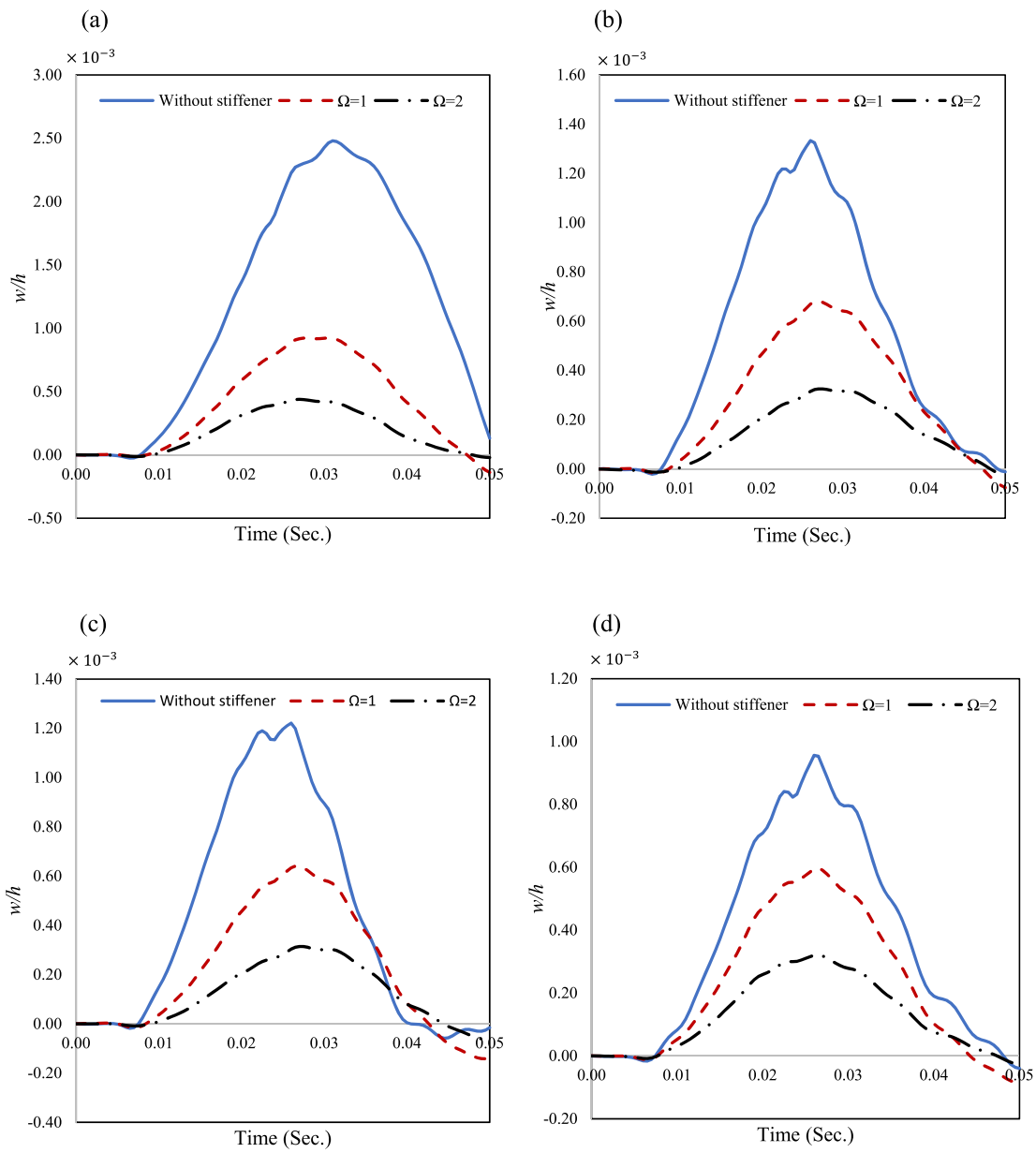

Fig. 18. Dimensionless deflections at the center of the unstiffened/stiffened 2D-FG plate with unevenly distributed porosities under a moving load in different boundary conditions ($\alpha_p = 0.1$, $n = m = 1$, $v = 20$ m/s): (a) SSSS, (b) SCSC, (c) SCCC, (d) CCCC.

The non-dimensional maximum central deflections ($w_{\max}/h$) of a bi-directional FG plate without porosity and stiffener under a moving load with a speed of 12 m/s for SSSS and CCCC boundary conditions are shown in Fig. 15. For both types of edge conditions, it is evident in Fig. 15 that the dimensionless dynamic deflections of the plates increase with growth in thickness and length (see FG indices (n, m)). However, the influence of the index (m) is much greater when the plate edges are clamped or $n \geq 2$.

Figs. 16 and 17, respectively, display the magnitude of w/h for an unstiffened/stiffened SCSC bidirectional FG plate with even and uneven distribution of porosities. This plate is supposed to a moving load with the velocity of 18 m/s. It is seen that with a rise in gradient terms n and m, the presence of the stiffener can be more pronounced in decreasing the values of w/h for every porosity distribution pattern. In the case of an evenly distributed porosity, for example, the reduction of peak deflection of the porous plate with $\alpha_p = 0.1$ and $(n, m) = (4, 4)$ due to a stiffener with depth ratio (Ω) of 1 is approximately 35% larger than that of its counterpart with $\alpha_p = 0.1$ and $(n, m) = (4, 2)$. Moreover, when it comes to such plates with porosity fraction of 0.2, this percentage become more, nearly 65%, Fig. 16(b). However, these percentages decrease significantly when the plates with uneven porosity distributions are used, Fig. 17.

Fig. 18 shows how much the longitudinal stiffener affects the transient deflections (w/h) of a porous 2D-FG plate $(n = m = 1)$ subjected to a moving load of 20 m/s for different boundary conditions. The main result obtained here is that simply supported boundary condition (SSSS) offers the greatest effect on reducing dimensionless dynamic displacements in all stiffener's depth ratios (Ω). For example, the stiffener with depth ratio (Ω) of 1 reduces deflection of the fully simply supported plate with no stiffeners about 63%, whereas for the SCSC, SCCC and fully clamped (CCCC) ones it is in the vicinity of 49%, 47% and 37%, respectively. Fig. 18 also illustrates that the further reduction in the plate can happen when Ω increases from 1 to 2. However, the difference between deflections of every stage in this rise ($\Omega = 0$ to

Table 3
Dimensionless maximum deflection of the porous plate with/without stiffeners under a moving load with constant velocity.

Type of plates	Porosity fraction	Gradient indexes (n, m)	$w_{max}/h \times 1000$							
			velocities							
			11 m/s	16 m/s	22 m/s	23 m/s	27 m/s	31 m/s	35 m/s	40 m/s
Unstiffened plates	$\alpha_p = 0$	(0.5, 0.5)	1.45	1.78	1.84	1.89	1.79	1.72	1.687	1.65
		(2, 2)	2.42	2.75	2.69	2.65	2.58	2.521	2.456	2.367
	$\alpha_p = 0.1$ (even pattern)	(0.5, 0.5)	1.65	2.07	2.20	2.11	2.08	2.02	1.96	1.91
		(2, 2)	3.42	3.67	3.48	3.47	3.38	3.34	3.20	2.93
	$\alpha_p = 0.1$ (uneven pattern)	(0.5, 0.5)	1.48	1.92	1.95	1.953	1.947	1.89	1.884	1.85
		(2, 2)	2.59	2.94	2.92	2.91	2.83	2.81	2.71	2.64
Stiffened plates ($\Omega = 1$)	$\alpha_p = 0$	(0.5, 0.5)	0.73	0.745	0.767	0.775	0.812	0.815	0.78	0.76
		(2, 2)	0.87	1.024	1.038	1.04	1.052	0.978	0.975	0.934
	$\alpha_p = 0.1$ (even pattern)	(0.5, 0.5)	0.84	0.85	0.82	0.84	0.94	1.02	0.90	0.82
		(2, 2)	1.08	1.22	1.17	1.22	1.254	1.20	1.12	1.07
	$\alpha_p = 0.1$ (uneven pattern)	(0.5, 0.5)	0.78	0.768	0.782	0.798	0.861	0.881	0.812	0.762
		(2, 2)	0.92	1.08	1.11	1.12	1.14	1.04	1.01	0.98

$\Omega = 1$ and $\Omega = 1$ to $\Omega = 2$) is to decline compared to the previous one.

The dimensionless maximum central deflections obtained by a moving load on the porous 2D-FG plate for simply supported boundary condition with a varying value of velocity are given in Table 3. It is seen that the maximum deflections at the center of the plate increase as long as the critical velocity is obtained, when the deflections reach their maximal values; after that they decline by speeding up the load. As depicted, for all cases, the critical velocities drop by increasing gradient indexes (n, m). It is also evident that when the plates are reinforced by the stiffener, the magnitudes of critical velocity increase since the stiffener enhances the stiffness of the structure.

5. Conclusions

Dynamic behaviors of stiffened porous 2D-FG plates with porosities distributed evenly or unevenly throughout the thickness of the plates under moving loads for different boundary conditions were investigated through employing the dynamic relaxation with kinetic damping (K-DR) and Newmark integration solving methods for the first time. In accordance with FSDT and the von Karman theory for large deflections, the nonlinear dynamic equations were developed after which, the effects of some parameters including material gradient indexes, porosity distribution patterns, stiffener depth to the plate ratio and type of boundary conditions on the transient responses of porous 2D-FG plates were studied. Some remarkable inferences are summarized as follows:

- Compared to the dynamic relaxation method with the viscos damping, K-DR procedure is more efficient and consumes less computational time. Hence, this improvement can be more noticeable in severe nonlinear behaviors.
- Material gradient indices (n, m) have a significant effect on the response of the plates; the axial FG index (m) has a greater effect on clamped than simply supported plates.
- Fully simply supported boundary conditions lead to less magnitudes of nonlinear frequency compared to that of SCSC.
- At the same porosity coefficient (fraction) and gradient index, the dimensionless maximum deflection for uneven distribution is smaller than the one for an even distribution.
- In the presence of the stiffener, the dynamic deflections decline enormously, while the values of critical velocity have dramatic increases. It means that using of stiffener not only can result in enhancing the strength of structures but also increase the nonlinear frequency.
- The reinforcing effect of the stiffeners is much noticeable in 2D-FG plates with higher material grading indexes (n, m) and porosity coefficients (fractions).
- The effect of the stiffeners on reduction of deflection increases by decreasing constrains on the plate boundary conditions.

Declaration of competing interest

The authors declare that they have no conflict of interest.

References

[1] T. Van Do, D.K. Nguyen, N.D. Duc, D. Hong Doan, T. Quoc Bui, Analysis of bi-directional functionally graded plates by FEM and a new third-order shear deformation plate theory, Thin-Walled Struct. 119 (2017) 687–699.

[2] M. Koizumi, FGM activities in Japan, Composites, Part B, Eng. 28B (1997) 1–4.

[3] N.D. Duc (Ed.), Nonlinear Static and Dynamic Stability of Functionally Graded Plates and Shells, Vietnam National University Press, Hanoi, 2014.

[4] T.M. Tu, T.H. Quoc, N. van Long, Vibration analysis of functionally graded plates using the eight-unknown higher order shear deformation theory in thermal environments, Aerosp. Sci. Technol. 84 (2019) 698–711, https://doi.org/10.1016/j.ast.2018.11.010.

[5] N.D. Duc, T.Q. Quan, Nonlinear stability analysis of double-curved shallow FGM panels on elastic foundations in thermal environments, Mech. Compos. Mater. 48 (4) (2012) 435–448, https://doi.org/10.1007/s11029-012-9289-z.

[6] Y.Q. Wang, J.W. Zu, Nonlinear steady-state responses of longitudinally traveling functionally graded material plates in contact with liquid, Compos. Struct. 164 (2017) 130–144, https://doi.org/10.1016/j.compstruct.2016.12.053.

[7] N.D. Duc, D.H. Bich, P.H. Cong, Nonlinear thermal dynamic response of shear deformable FGM plates on elastic foundations, J. Therm. Stresses 39 (3) (2016) 278–297.

[8] N.D. Duc, Nonlinear thermo-electro-mechanical dynamic response of shear deformable piezoelectric sigmoid functionally graded sandwich circular cylindrical shells on elastic foundations, J. Sandw. Struct. Mater. 20 (3) (2016) 351–378.

[9] M. Adineh, M. Kadkhodayan, Three-dimensional thermo-elastic analysis and dynamic response of a multi-directional functionally graded skew plate on elastic foundation, Composites, Part B, Eng. 125 (2017) 227–240.

[10] M. Nemat-Alla, Reduction of thermal stresses by developing two-dimensional functionally graded materials, Int. J. Solids Struct. 40 (2003) 7339–7356.

[11] L. Li, R. Xiaohui, Stiffened plate bending analysis in terms of refined triangular laminated plate element, Compos. Struct. 92 (2010) 2936–2945.

[12] M. Nemat-Alla, K.I. Ahmedi, b. Hassab-Allah, Elastic–plastic analysis of two-dimensional functionally graded materials under thermal loading, Int. J. Solids Struct. 46 (2009) 2774–2786.

[13] M.J. Ebrahimi, M.M. Najafizadeh, Free vibration analysis of two-dimensional functionally graded cylindrical shells, Appl. Math. Model. 38 (2014) 308–324.

[14] S. Satouri, K.M.F. Allahkarami, A. Asanjarani, Application of third order shear deformation theory in buckling analysis of 2D-functionally graded cylindrical shell reinforced by axial stiffeners, Composites, Part B, Eng. 59 (2015) 236–253.

[15] L. Li, H. Yujin, Torsional vibration of bi-directional functionally graded nanotubes based on nonlocal elasticity theory, Compos. Struct. 15 (2017) 242–250.

[16] M. Zamani, H. Nejadamin, Non-local analysis of free vibration of bi-directional functionally graded Euler–Bernoulli nano-beams, Int. J. Eng. Sci. 105 (2016) 1–11.

[17] B. Kieback, A. Neubrand, A. Riedel, Processing techniques for functionally graded materials, Mater. Sci. Eng. A 362 (2003) 81–105.
[18] Y.Q. Wang, J.W. Zu, Vibration characteristics of moving sigmoid functionally graded plates containing porosities, Int. J. Mech. Mater. Des. 14 (4) (2018) 473–489.
[19] D. Chen, J. Yang, A. Chaikittiratana, Elastic buckling and static bending of shear deformable functionally graded porous beam, Compos. Struct. 133 (2015) 54–61.
[20] J. Zhu, Z. Lai, Z. Yin, J. Jeon, S. Lee, Fabrication of ZrO_2–NiCr functionally graded material by powder metallurgy, Mater. Chem. Phys. 68 (2001) 130–135.
[21] Y.Q. Wang, Z. Yang, Nonlinear vibrations of moving functionally graded plates containing porosities and contacting with liquid: internal resonance, Nonlinear Dyn. 90 (2) (2017) 1461–1480, https://doi.org/10.1007/s11071-017-3739-z.
[22] Y.Q. Wang, J.W. Zu, Vibration behaviors of functionally graded rectangular plates with porosities and moving in thermal environment, Aerosp. Sci. Technol. 69 (2017) 550–562, https://doi.org/10.1016/j.ast.2017.07.023.
[23] Nguyen Dinh Duc, Vu Dinh Quang, Pham Dinh Nguyen, Trinh Minh Chie, Nonlinear dynamic response of functionally graded porous plates on elastic foundation subjected to thermal and mechanical loads, J. Appl. Comput. Mech. 4 (4) (2018) 245–259.
[24] N.D. Duc, Nonlinear dynamic response of imperfect eccentrically stiffened FGM double curved shallow shells on elastic foundation, Compos. Struct. 99 (2013) 88–96, https://doi.org/10.1016/j.compstruct.2012.11.017.
[25] N.D. Duc, T.Q. Quan, Nonlinear response of imperfect eccentrically stiffened FGM cylindrical panels on elastic foundation subjected to mechanical loads, Eur. J. Mech. A, Solids 46 (2014) 60–71, https://doi.org/10.1016/j.euromechsol.2014.02.005.
[26] N. Ziane, S.A. Meftah, G. Ruta, A. Tounsi, Thermal effects on the instabilities of porous FGM box beams, Eng. Struct. 134 (2017) 150–158.
[27] Y.Q. Wang, Electro-mechanical vibration analysis of functionally graded piezoelectric porous plates in the translation state, Acta Astronaut. 143 (2018) 263–271.
[28] P.H. Cong, T.M. Chien, N. Dinh Khoa, N. Dinh Duc, Nonlinear thermomechanical buckling and post-buckling response of porous FGM plates using Reddy's HSDT, Aerosp. Sci. Technol. 77 (2018) 419–428.
[29] Y. Wang, C. Ye, J.W. Zu, Identifying the temperature effect on the vibrations of functionally graded cylindrical shells with porosities, Appl. Math. Mech. (English Ed.) 39 (11) (2018) 1587–1604, https://doi.org/10.1007/s10483-018-2388-6.
[30] P.T. Thang, T. Nguyen-Thoi, D. Lee, J. Kang, J. Lee, Elastic buckling and free vibration analyses of porous-cellular plates with uniform and non-uniform porosity distributions, Aerosp. Sci. Technol. 79 (2018) 278–287, https://doi.org/10.1016/j.ast.2018.06.010.
[31] D. Shahsavari, M. Shahsavari, L. Li, B. Karami, A novel quasi-3D hyperbolic theory for free vibration of FG plates with porosities resting on Winkler/Pasternak/Kerr foundation, Aerosp. Sci. Technol. 72 (2018) 134–149.
[32] N. Wattanasakulpong, A. Chaikittiratana, On the linear and nonlinear vibration responses of elastically end restrained beams using DTM, Mech. Based Des. Struct. Mach. 42 (2014) 135–150.
[33] H. Tang, L. Li, Y. Hu, Buckling analysis of two-directionally porous beam, Aerosp. Sci. Technol. 78 (2018) 471–479.
[34] H. Lamb, On the propagation of tremors over the surface of an elastic solid, Philos. Trans. R. Soc. A 203 (359–371) (1904) 1–42, https://doi.org/10.1098/rsta.1904.0013.
[35] E. Wilson, A. Tsrik, Dynamic Behavior of Rectangular Plates and Cylindrical Shell, New York University, 1967.
[36] O.P. Agrawal, M.M. Stanišić, S. Saigal, Dynamic responses of orthotropic plates under moving masses, Ing.-Arch. 58 (1) (1988) 9–14.
[37] S. Marchesiello, A. Fasana, L. Garibaldi, B. Piombo, Dynamics of multi-span continuous straight bridges subject to multi-degrees of freedom moving vehicle excitation, J. Sound Vib. 224 (3) (1999) 541–561, https://doi.org/10.1006/jsvi.1999.2197.
[38] A.R. de Faria, D. Oguamanam, Finite element analysis of the dynamic response of plates under traversing loads using adaptive meshes, Thin-Walled Struct. 42 (10) (2004) 1481–1493, https://doi.org/10.1016/j.tws.2004.03.012.
[39] A.R. Vosoughi, P. Malekzadeh, H. Razi, Response of moderately thick laminated composite plates on elastic foundation subjected to moving load, Compos. Struct. 97 (2013) 286–295, https://doi.org/10.1016/j.compstruct.2012.10.017.
[40] P. Malekzadeh, S.M. Monajjemzadeh, Nonlinear response of functionally graded plates under moving load, Thin-Walled Struct. 96 (2015) 120–129, https://doi.org/10.1016/j.tws.2015.07.017.
[41] P. Malekzadeh, S.A. Shojaee, Dynamic response of functionally graded plates under moving heat source, Composites, Part B, Eng. 44 (1) (2013) 295–303.
[42] M. Şimşek, M. Aydın, Size-dependent forced vibration of an imperfect functionally graded (FG) microplate with porosities subjected to a moving load using the modified couple stress theory, Compos. Struct. 160 (2017) 408–421.
[43] A. Golzari, M. Asgari, Dynamic analysis and wave propagation in rotating heterogeneous cylinders under moving load and thermal conditions; implementing an efficient mesh free method, Appl. Math. Model. 61 (2018) 377–407, https://doi.org/10.1016/j.apm.2018.05.001.
[44] Y. Yang, K. Kunpang, C. Lam, V. Iu, Dynamic behaviors of tapered bi-directional functionally graded beams with various boundary conditions under action of a moving harmonic load, Eng. Anal. Bound. Elem. 104 (2019) 225–239.
[45] N.D. Duc, Q.Q. Tran, D.K. Nguyen, New approach to investigate nonlinear dynamic response and vibration of imperfect functionally graded carbon nanotube reinforced composite double curved shallow shells subjected to blast load and temperature, Aerosp. Sci. Technol. 71 (2017) 360–372.
[46] N. van Thanh, N.D. Khoa, N.D. Tuan, P. Tran, N.D. Duc, Nonlinear dynamic response and vibration of functionally graded carbon nanotube-reinforced composite (FG-CNTRC) shear deformable plates with temperature-dependent material properties and surrounded on elastic foundations, J. Therm. Stresses 40 (10) (2017) 1254–1274.
[47] Y.Q. Wang, C. Ye, J.W. Zu, Nonlinear vibration of metal foam cylindrical shells reinforced with graphene platelets, Aerosp. Sci. Technol. 85 (2019) 359–370.
[48] G.J. Turvey, N. Der Avanessian, Axisymmetric elasto-plastic large deflection response of ring stiffened circular plates, Int. J. Mech. Sci. 31 (11–12) (1989) 905–924.
[49] M.E. Golmakani, M. Kadkhodayan, Large deflection thermoelastic analysis of functionally graded stiffened annular sector plates, Int. J. Mech. Sci. 69 (2013) 94–106.
[50] M. Mehrabian, M.E. Golmakani, Nonlinear bending analysis of radial-stiffened annular laminated sector plates with dynamic relaxation method, Comput. Math. Appl. 69 (2015) 1272–1302.
[51] M.E. Golmakani, M. Emami, Buckling and large deflection behaviors of radially functionally graded ring-stiffened circular plates with various boundary conditions, Appl. Math. Mech. 37 (2016) 1131–1152.
[52] N.D. Duc, T.Q. Quan, Nonlinear postbuckling of imperfect eccentrically stiffened P-FGM double curved thin shallow shells on elastic foundations in thermal environments, Compos. Struct. 106 (2013) 590–600.
[53] N.D. Duc, Nonlinear thermal dynamic analysis of eccentrically stiffened S-FGM circular cylindrical shells surrounded on elastic foundations using the Reddy's third-order shear deformation shell theory, Eur. J. Mech. A, Solids 58 (2016) 10–30, https://doi.org/10.1016/j.euromechsol.2016.01.004.
[54] M. Taczała, R. Buczkowski, M. Kleiber, Nonlinear buckling and post-buckling response of stiffened FGM plates in thermal environments, Composites, Part B, Eng. 109 (2017) 238–247.
[55] P.M. Vuong, N.D. Duc, Nonlinear response and buckling analysis of eccentrically stiffened FGM toroidal shell segments in thermal environment, Aerosp. Sci. Technol. 79 (2018) 383–398.
[56] N.D. Duc, K. Seung-Eock, D.Q. Chan, Thermal buckling analysis of FGM sandwich truncated conical shells reinforced by FGM stiffeners resting on elastic foundations using FSDT, J. Therm. Stresses 41 (3) (2017) 331–365.
[57] N. Dinh Duc, P. Dinh Nguyen, N. Dinh Khoa, Nonlinear dynamic analysis and vibration of eccentrically stiffened S-FGM elliptical cylindrical shells surrounded on elastic foundations in thermal environments, Thin-Walled Struct. 117 (2017) 178–189.
[58] E. Allahyari, M. Asgari, A.A. Jafari, Nonlinear size-dependent vibration behavior of graphene nanoplate considering surfaces effects using a multiple-scale technique, Mech. Adv. Mat. Struct. (2018) 1–10.
[59] Y.Q. Wang, X.B. Huang, J. Li, Hydroelastic dynamic analysis of axially moving plates in continuous hot-dip galvanizing process, Int. J. Mech. Sci. 110 (2016) 201–216.
[60] Y.Q. Wang, Y.H. Wan, J.W. Zu, Nonlinear dynamic characteristics of functionally graded sandwich thin nanoshells conveying fluid incorporating surface stress influence, Thin-Walled Struct. 135 (2019) 537–547.
[61] Y.Q. Wang, Nonlinear vibration of a rotating laminated composite circular cylindrical shell: traveling wave vibration, Nonlinear Dyn. 77 (4) (2014) 1693–1707.
[62] L.L. Ke, J. Yang, S. Kitipornchai, An analytical study on the nonlinear vibration of functionally graded beams, Meccanica 45 (6) (2010) 743–752.
[63] Y. Tang, Q. Ding, Nonlinear vibration analysis of a bi-directional functionally graded beam under hygro-thermal loads, Compos. Struct. 225 (2019) 111076.
[64] Y.Q. Wang, L. Liang, X.H. Guo, Internal resonance of axially moving laminated circular cylindrical shells, J. Sound Vib. 332 (24) (2013) 6434–6450.
[65] A. Basu, P. Djahani, P. Dowling, Elastic post-buckling behavior of discretely stiffened plates, in: Colloquium on the Stability of Steel Structures, Liege, Belgium, 1977.
[66] J. Reddy, Energy and Vibrational Methods in Applied Mechanics, John Wiley and Sons, New York, 1984.
[67] M. Taheri, E. Ting, Dynamic response of plate to moving loads: structural impedance method, Compos. Struct. 33 (1989) 1379–1390.
[68] M. Koli, K. Chandrashekhara, Nonlinear static and dynamic analysis of stiffened laminated plate, Int. J. Non-Linear Mech. 32 (1997) 89–101.
[69] M. Rezaiee-Pajand, J. Alamatian, Implicit higher order accuracy method for numerical integration in dynamic analysis, J. Struct. Eng. 28 (2008) 973–985.
[70] M. Kadkhodayan, J. Alamatian, G. Turvey, A new fictitious time for the dynamic relaxation (DXDR) method, Int. J. Numer. Methods Eng. 74 (2008) 996–1018.
[71] B. Topping, P. Ivanyi, Computer Aided Design of Cable-Membrane Structures, Saxe-Coburg Publications on Computational Engineering, 2007.
[72] B. Topping, A. Khan, Parallel computation schemes for dynamic relaxation, Eng. Comput. 11 (1994) 513–548.

[73] J. Alamatian, A new formulation for fictitious mass of the dynamic relaxation method with kinetic damping, Comput. Struct. 90–91 (2012) 42–54.
[74] A. Rezaei Mojdehi, A. Darvizeh, A. Basti, H. Rajabi, Three dimensional static and dynamic analysis of thick functionally graded plates by the meshless local Petrov–Galerkin (MLPG) method, Eng. Anal. Bound. Elem. 35 (2011) 1168–1180.
[75] S.A. Eftekhari, A differential quadrature procedure with regularization of Dirac-delta-function for numerical solution of moving load problem, Lat. Am. J. Solids Struct. 12 (2014) 1241–1265.